On the Dissociation of van der Waals Clusters of X_2−Cyclohexane (X = O, Cl) Following Charge-Transfer Excitation in the Ultraviolet†

Bradley F. Parsons‡ and David W. Chandler*

Sandia National Laboratories, Combustion Research Facility, Livermore, California 94550

Received: January 27, 2003; In Final Form: April 25, 2003

We report the results of experiments investigating the charge-transfer state photofragments of a van der Waals cluster after excitation through a strong absorption band in the ultraviolet. The O_2−cyclohexane cluster has a strong absorption to a charge-transfer state near 226 nm resulting in dissociation yielding $O(^3P)$. On the basis of a simple model (Mulliken, R. S. *J. Am. Chem. Soc.* **1952**, *74*, 811) and low level ab initio calculations, the location of the charge-transfer absorption for a Cl_2−cyclohexane cluster is predicted and the dissociation of this cluster leading to $Cl^*(^2P_{1/2})$ and $Cl(^2P_{3/2})$ is also investigated. The translational energy distribution, $P(E_T)$ for each cluster is analyzed in terms of two possible dissociation mechanisms. The dissociation may be considered to proceed on the initially accessed charge-transfer state through a harpooning-type mechanism. Alternatively, the dissociation may proceed following a nonadiabatic electronic transition to the neutral excited states of the diatomic subunit of the cluster. For O_2−cyclohexane, the $P(E_T)$ is consistent with the second dissociation mechanism. We determine from the available data that the likely structure for the vdW complex is analogous to the resting structure of I_2−benzene with the O_2 bond axis lying above the cyclohexane ring. For Cl_2−cyclohexane, we analyze the velocity dependence of the Cl recoil anisotropy and find it increases from nearly isotropic ($\beta \sim 0$) to distinctly anisotropic ($\beta \sim 1.7-2$). The fast, anisotropic Cl atoms result from dissociation of the cluster on the neutral excited states of Cl_2. The slow, isotropic Cl atoms likely result from secondary dissociation of the product Cl−cyclohexane cluster. We determine a $Cl^*(^2P_{1/2})/Cl(^2P_{3/2})$ branching ratio of 0.53 ± 0.05 and estimate that ∼19% of the observed Cl atoms result from primary dissociation on the initially accessed charge-transfer state. The data suggest that the Cl_2−cyclohexane cluster has an axial-like structure following absorption of a photon. Finally, we explain the rapid nonadiabatic hop from the charge-transfer state to the neutral excited states of the diatomic in terms of coupling of the states though a one-electron change.

I. Introduction

Many atoms and molecules can form weak van der Waals complexes with well depths on the order of 100 cm^{-1} (0.3 kcal/mol) and many of these are capable of undergoing electron transfer (charge transfer) between the subunits following absorption of a photon. The classic example of such a complex is benzene−I_2 (Bz−I_2). The absorption spectrum of this complex shows an absorption feature at 297 nm in solution[1] and 268 nm in the gas phase[2] not due to either subunit. This absorption band was first explained by Mulliken[3] in the early 1950s. Mulliken considered the electronic structure of the complex in terms of a molecular wave function with contribution from a no-bond wave function, $\psi_{NB} = \psi_A\psi_D$ (where ψ_A and ψ_D are the ground-state wave functions for the acceptor and donor subunits of the cluster) and a dative wave function, $\psi_{Dat} = \psi(A^- \cdots D^+)$.[3,4] The molecular wave function from the ground-state electronic configuration is the sum of the no-bond and dative wave functions: $\psi_{gs} = a\psi_{NB} + b\psi_{Dat}$ and is dominated by the no-bond wave function ($a^2 \gg b^2$) while the wave function for the excited state is $\psi_{es} = a^*\psi_{NB} - b^*\psi_{Dat}$ and is dominated by the dative electronic configuration ($b^{*2} \gg a^{*2}$)[3]. Using these ideas along with second-order perturbation theory, Mulliken predicted oscillator strengths from these charge-transfer transitions in fair agreement with the experimentally observed values. Furthermore, he pointed out[3] that the energy for the charge-transfer absorption could be found by considering the subunits at infinite separation and adding the coulomb interaction:

$$E_{CT} = IP_D - EA_A - \frac{e^2}{R} \quad (1)$$

where IP_D is the ionization potential of the donor, EA_A is the electron affinity of the acceptor, and e^2/R is the cation/anion Coulomb interaction.

Following absorption to the charge-transfer state, many of the clusters dissociate to yield atomic fragments.[5−11] Typically, the complex may dissociate along two different pathways. First, the dissociation may take place on the initially accessed charge-transfer state to yield an atomic product, while the organic cation harpoons the atomic negative ion in the exit channel, eq 2:

$$D-A_2 \xrightarrow{h\nu} D^+-A_2^- \xrightarrow{\text{diss}} D^+-A^- + A \quad (2)$$

Alternatively, the diatomic anion can return an electron (though not necessarily the electron it initially received) to the organic cation, placing the diatomic on one of its neutral excited states where the dissociation proceeds, eq 3:

$$D-A_2 \xrightarrow{h\nu} D^+-A_2^- \xrightarrow{e} D^*-A^*_2 \xrightarrow{\text{diss}} D^*-A + A \quad (3)$$

† Part of the special issue "Charles S. Parmenter Festschrift".

* Corresponding author. E-mail: chand@sandia.gov.
‡ E-mail: bfparso@sandia.gov.

10.1021/jp0301150 CCC: $25.00
Published on Web 07/23/2003

Considerable experimental work has been devoted to the Bz−I_2 system, which serves as a model for the dissociation of charge-transfer clusters. In particular, Zewail and co-workers[5,6,11] studied Bz−I_2 with excitation near 270 nm. They initially determined the I atom appearance time (τ)[5,11] from this system to be ∼750 fs. This fast appearance time (τ < 1 ps) implied a prompt dissociation, which was interpreted as resulting from the initially accessed charge-transfer state, eq 2. However, later work[6] coupling ultrafast detection with kinetic energy resolved time-of-flight (KETOF) detection showed two I atom channels, each with a different appearance time and recoil anisotropy. The experiments indicated that the charge-transfer (CT) state decayed in ∼200 fs while molecular dynamics simulations indicated the CT dissociation should take place in ∼2 ps. The resulting I atoms were assigned to dissociation on the neutral excited states of I_2, eq 3. The two channels were assigned as fast uncaged I atoms (those directed away from the ring in an axial structure with the I−I bond axis oriented along the C_6 symmetry axis of benzene) with a rapid appearance time ($\tau \sim$ 450 fs) and an anisotropic angular distribution ($\beta \sim 0.7-1$) and slow caged I atoms (directed toward the ring) with a slow appearance time ($\tau \sim 1.4$ ps) and nearly isotropic product angular distribution ($\beta \sim 0.2-0.3$). The anisotropy parameter for the fast channel is considerably reduced from the limiting value of $\beta = 2$, indicating the clusters undergo large amplitude torsional motion on the vdW state.[6]

Young and co-workers[10] also investigated the dissociation of I_2−Bz near 270 nm using KETOF. They too observed two I atom channels originating from dissociation on the neutral excited states of I_2 following the mechanism in eq 3 with the fast, anisotropic channel resulting from uncaged I atoms while the slow isotropic channel result from caged I atoms. They concluded[10] that the dissociation occurs from an oblique I_2−Bz structure with the I−I bond axis tilted ∼35° from the C_6 symmetry axis. Young and co-workers[9] also determine the Bz rotational temperature following dissociation of the cluster to be $T_{rot} \sim 1500$ K, implying high rotational excitation during the dissociation.

In addition to Bz−I_2 complexes, several other organic−diatomic complexes have been investigated in recent years. Grover et al.[12] studied clusters of O_2 with benzene and several derivatives. They determined dissociation energies (D_0) of the clusters as ∼1.5−2 kcal/mol, implying a van der Waals-type interaction in the ground state. DeBoer and Young[7] investigated the dissociation of Bz−O_2 complexes to give atomic oxygen following excitation at 226 nm. They considered both of the dissociation mechanisms detailed above. To consider the possibility of dissociation according to a harpooning mechanism, eq 2, the ground state of the molecular oxygen anion, O_2^- was shifted up by the calculated charge-transfer energy from eq 1 assuming a charge-transfer dipole length of 3.3 Å.[7,8] The total energy available for this single-photon dissociation is $E_{photon} =$ 5.6 eV; however, the asymptotic limit for the products of the dissociation on the charge-transfer state is 8.6 eV. DeBoer et al. argued that the dissociation could take place on this state noting that Maslen et al.[13] observed a lowering of the asymptotic energy due to coupling of the degenerate wave functions by local electric fields. It is worth noting, however, that the data measured by DeBoer and Young for the dissociation of the Bz−O_2 complex at 226 nm is in excellent agreement with the expected energetic limit for dissociation on the neutral excited states of O_2 since the maximum energy that may be partitioned into translation may be found from the available energy:

$$E_{avail} = E_{photon} - D_0(O_2) + E_{int} \quad (4)$$

Neglecting the contribution of E_{int} (since the molecular beam is cold enough to generate vdW clusters, this approximation should be a valid), then the available energy is 8.8 kcal/mol, so the maximum O atom recoil kinetic energy is 7.6 kcal/mol in the center-of-mass reference frame. Indeed, DeBoer and Young[7] determined a $P(E)$ for the O fragment that extends to near the energetic limit and peaks at very low kinetic energy (∼0.5 kcal/mol) with an isotropic product angular distribution. This observation is consistent with a statistical dissociation with a very small or no barrier in the exit channel, as would be expected for dissociation following a nonadiabatic transition to one of the weakly repulsive excited states of oxygen. More recently, Young and co-workers[14] have investigated the fragmentation of O_2−alkene (ethene, propene, 1-butene, *cis*- and *trans*-2-butene, 2-methylpropene, 2-methyl-2-butene, and 2,3-dimethyl-2-butene) complexes at 226 nm both experimentally and theoretically. Similar to O_2−benzene, excitation at 226 nm results in the production of $O(^3P_j)$ fragments with an isotropic angular distribution and low recoil velocities. The clusters dissociate following reverse electron transfer (though not the same electron) returning O_2^- to a neutral excited state of O_2.

Guidoni et al.[15] studied the fragmentation of several charge-transfer complexes between molecular oxygen and various donor molecules (benzene, toluene, cyclohexane, butane, methane, and methanol in addition to water, xenon, krypton, and argon). An enhancement of the $O(^3P_j)$ signal, detected using 2 + 1 REMPI at 226 nm, was found when a small fraction of the donor was seeded in the molecular beam. Of particular interest to the present study was the observation of a strong O-atom signal following excitation and resonant ionization at 226 nm for the O_2−cyclohexane complex.[15] Guidoni et al. also investigated the partitioning of oxygen atom fine structure levels $O(^3P_j)$ $j = 0,1,2$ and found statistical populations.

We have investigated the dissociation of the O_2−cyclohexane van der Waals complex at 226 nm. Furthermore, we have investigated dissociation of the charge-transfer cluster, Cl_2−cyclohexane, at 240 nm. The ion image of the atomic fragment from the dissociation of either complex is recorded using a linearly polarized laser beam. From the ion image, we extract the center-of-mass recoil kinetic energy distribution of the dissociating cluster and compare this with the calculated translational energy release for dissociation on either the initially accessed charge-transfer state or the neutral excited states of the diatomic acceptor. In the next section, we give a brief description of the experimental setup. We then discuss some low level ab initio calculations that predict the structure and binding energy for these vdW clusters. In the fourth section, we present the ion images obtained for both systems and discuss how we extract a recoil kinetic energy distribution from these images. In the fifth section of this paper, the $P(E_T)$ for both systems are analyzed in terms of the dissociation mechanisms outlined above. The final section provides a summary of the results and interpretations of the data presented in this paper.

II. Experimental Section

These experiments were carried out in a unimolecular ion imaging apparatus with a molecular beam directed toward the face of the two-dimensional position sensitive detector. A mixture of O_2 (∼5%) with cyclohexane (Cy, ∼1%) in He was introduced into the source region of the vacuum chamber (base pressure during experiments $\sim 5 \times 10^{-5}$ Torr) through a General

Valve Series 9 pulsed valve (750 μm orifice) with a backing pressure of ~40 psig. The supersonic molecular beam was skimmed once using a 700 μm diameter skimmer and passed through a 1.5 mm hole on the repeller of the ion optic assembly. Experiments on Cl_2−cyclohexane clusters were conducted in a similar manner using a dilute Cl_2/Cy/He beam.

The molecular beam was crossed approximately 10 cm downstream from the nozzle by the photolysis/REMPI probe laser. Photolysis/probe photons are obtained by frequency doubling the output of a dye laser (SpectraPhysics Sirah) pumped by the third harmonic of an injection-seeded Nd:YAG laser (QuantaRay PRO-290) operating at a repetition rate of 30 Hz. The dye laser was operated with either Coumarin 450 (Exciton) or Coumarin 480 (Exciton) to generate light near 451 or 481 nm, respectively. The dye laser fundamental is frequency doubled in BBO (Inrad) to generate photolysis and REMPI photons, which were focused at the interaction region using an $f = 14$ in. lens.

To determine the $Cl^*(^2P_{1/2})/Cl(^2P_{3/2})$ branching ratio from the Cl_2−Cy cluster, we photolyze Cl_2 at 425 nm and calibrate our experimental detection efficiency. A molecular beam of 5% Cl_2 in He is introduced into the source region of the vacuum chamber and photolyzed using the fundamental output of a dye laser (Lambda Physik, Scanmate) pumped by the third harmonic of an Nd:YAG laser (Coherent Infinity) operating at 30 Hz. The Cl probe pulse is the same as that used to detect Cl atoms for Cl_2−cyclohexane.

III. Ab-Initio Results

Ab-initio electronic structure calculations are performed using Gaussian 98[16] to predict the equilibrium structure and well depth for O_2−Cy and Cl_2−Cy as well as the clusters formed between cyclohexane and either atomic oxygen or atomic chlorine. Geometries are first optimized at the B3LYP level of theory using a 6-31g(d) basis set. The optimized structures for the vdW clusters appear in Figure 1. Table 1 gives the energy (in atomic units) at this level of theory for all four X−Cy clusters (X = O_2, Cl_2, O, Cl) as well as the energy for the separated species (O_2, Cl_2, O, Cl, Cy). We also give the separation between the subunits of the vdW clusters and the well depth (D_e) for the clusters. Gaussian 98 predicts two bound cluster geometries for O_2−cyclohexane. The higher energy structure, Figure 1a, ($D_e \sim 141$ cm^{-1}) places the O_2 bond axis along the C_3 symmetry axis of the cyclohexane ring and is analogous to the axial structure of I_2−Bz[17] with a center-to-center separation of $R =$ 4.6 Å. However, this structure has a single imaginary frequency corresponding to O_2 torsional motion making it a first-order top and not a true global minimum. The lower energy structure (Figure 1b) places the O_2 bond axis above the ring similar to the resting structure of I_2−Bz[17] with a center-to-center separation of $R = 4.1$ Å and a binding energy of $D_e \sim 239$ cm^{-1}. This structure has a positive definite Hessian and is the structure of the cluster at the global minimum. Inserting the calculated separation into eq 1 along with the vertical ionization potential of cyclohexane (IP = 10.3 eV)[18] and the electron affinity of O_2 (EA = 0.45 eV)[19] predicts the absorption maximum for the charge-transfer state as $E_{CT} = 6.3$ eV for the global minimum structure (Figure 1b).

We plot a qualitative potential energy surface for the charge-transfer complex in a manner similar to that used in other investigations.[6,7] The ground state of the negative ion is shifted up by a constant energy; Cheng et al. and DeBoer and Young use different methods to find the shift energy. Cheng et al. shift

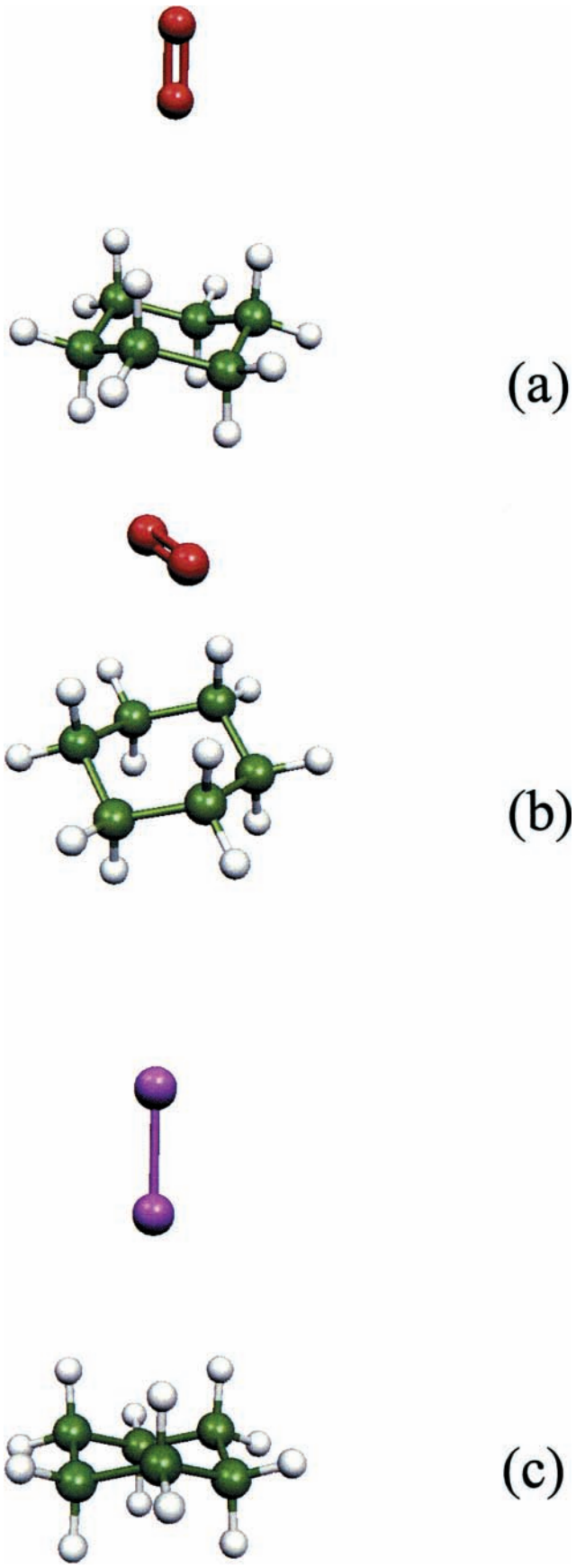

Figure 1. Geometries of cyclohexane−X_2 van der Waals clusters. The top frame shows the axial structure of O_2−Cy. The middle frame shows the resting O_2−Cy structure and the bottom frame shows the Cl_2−cyclohexane axial structure. All geometries are minimized at the B3LYP/6-31g(d) level using Gaussian 98 (see description in text).

TABLE 1: Calculated Parameters for the Charge-Transfer Clusters and the Subunits

	B3LYP/6-31g(d)[a]	R_{DA}[b]	E_{CT}[c]	$E_{cluster}$[d]
O_2−Cy	−386.2015923[e]	4.56[e]	6.7[e]	239[e]
	−386.2011529	4.1	6.3	141
Cl_2−Cy	−1156.2308017	5.1	4.94	101
O−Cy	−310.9433248	3.35	4.5	494
Cl−Cy	−696.025358	3.60	2.65	1896
O_2	−150.3200421			
Cl_2	−920.3498845			
O	−75.0606115			
Cl	−460.1362559			
Cy	−235.8804627			

[a] Energy in atomic units. [b] The charge-transfer bond length (in units of Å) at the B3LYP/6-31g(d) level. [c] Predicted absorption maximum (in eV) using eq 1 and the calculated donor−acceptor separation. [d] The cluster binding energy in units of cm^{-1}. [e] Energy for resting structure.

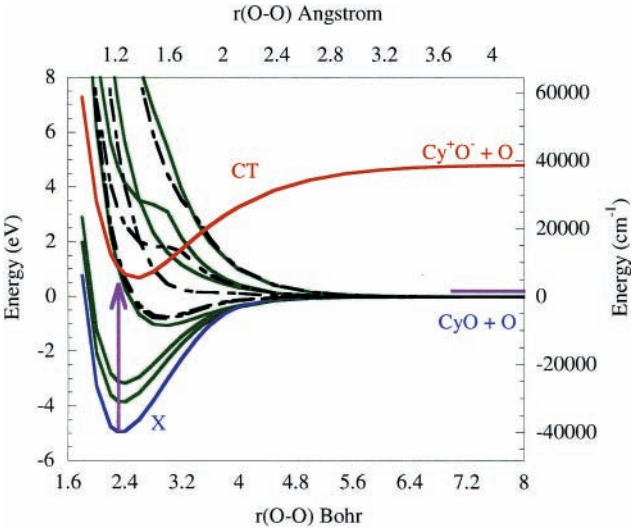

Figure 2. Potential energy surfaces for the O_2 ground state and the neutral excited states of O_2 (green solid: triplet, black dash: singlet) correlating with 2 O(^{3}P) fragments. Also depicted in red is the charge-transfer state of the cluster (shifted O_2^- ground state). The charge-transfer state is therefore *bound* by about 4.6 eV while the neutral excited states of O_2 are *unbound* by about 0.38 eV. Finally, the purple line shows the energy of the photon relative to the bottom of the O_2 ground-state PES.

the ground state of I_2^- such that the asymptotic energy matches that of the products ($Bz^+I^- + I$) while DeBoer and Young shift the ground state of O_2^- by the energy of the charge-transfer state. Both methods give similar results; however, simply shifting the ground-state anionic potential of the diatom does not account for the coulomb interaction between the O^- and Cy^+ products after dissociation on the charge-transfer state. Therefore, we calculate the shift energy to agree at the asymptote by estimating the energy of these CT clusters formed as products using eq 1. The vertical shift energy is

$$E_{shift} = E_{CT,Cy-O} + \Delta H_{f,O} + EA_{O_2} = IP_{Cy} - EA_O - e^2/R + \Delta H_{f,O} + EA_{O_2} \quad (5)$$

The first term in eq 5 is the energy of the Cy^+O^- charge-transfer state, and the second term is the heat of formation for the atom (the asymptotic energy of the products above the ground state of the neutral diatomic). The final term in eq 5 accounts for the energy difference between the ground state of the neutral diatom and the ground state of the anionic diatom. Figure 2 shows a plot of the charge-transfer state (shifted anionic ground state)

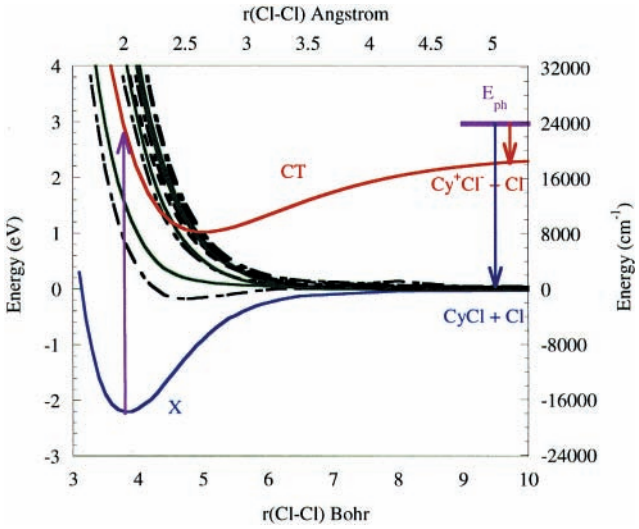

Figure 3. Potential energy surfaces for the Cl_2 ground state and the neutral excited states of Cl_2 (green solid: triplet, black dash: singlet) correlating with 2 Cl(^{2}P) fragments.[24] The initially accessed charge-transfer state (shifted Cl_2^- ground state) is shown in red. The maximum available energy for dissociation on the initially accessed charge-transfer state (red arrow) is about 13 kcal/mol, while the maximum available energy for dissociation on the neutral excited state of Cl_2 (blue arrow) is about 62 kcal/mol. The energy of the photon relative to the bottom of the Cl_2 ground state is shown in purple.

along with the ground state of O_2 and the neutral excited states of O_2 correlating with ground-state products. The ground state and neutral excited state of O_2 are taken from reference 20 while the anionic ground state is fit to a Morse potential using the parameters found in reference 21. The arrow gives the energy of the photon, and the thick line above the asymptotic limit of the neutral excited state shows the energy of the photon referenced to the bottom of the O_2 ground state. The initially accessed charge-transfer state is therefore bound by about 4.6 eV, while the neutral excited states of O_2 are unbound with total available energy, $E_{avail} = 0.38$ eV $= 8.8$ kcal/mol.

We have also performed electronic structure calculations to predict the structure of the Cl_2−cyclohexane cluster; the results of these calculations also appear in Table 1. The B3LYP/6-31g(d) optimized geometry for the Cl_2−Cy cluster is shown in Figure 1c. Gaussian 98 predicts a minimum only for the axial structure for Cl_2−cyclohexane at this level of theory with a binding energy of $D_e \sim 101$ cm^{-1} and a center-to-center separation of $R = 5.1$ Å. Inserting this separation along with the electron affinity of Cl_2 (EA = 2.5 eV)[22] into eq 1 predicts the energy of the charge-transfer state to be 4.9 eV corresponding to an absorption peak only 0.25 eV red of the 2 + 1 REMPI scheme for Cl($^2P_{3/2}$) and Cl*($^2P_{1/2}$) near 240 nm.[23] Thus, we predict that the charge-transfer state of the Cl_2−Cy cluster can be excited with a 240 nm photon, which can also probe the Cl fragments from the dissociation. Figure 3 shows the ground state and both the singlet (solid) and triplet (dashed) neutral excited states of Cl_2 correlating with 2 Cl(^{2}P) fragments taken from reference 24. We also show an approximate potential energy surface for the charge-transfer state by shifting a Morse potential fit for the ground state of the Cl_2 negative ion[25] to agree with the asymptotic product energies (we estimate the *maximum* coulomb interaction for the Cl^-−Cy^+ cluster assuming spherical Cl^- (with known anionic radius) in close contact with the Cy^+ structure from our calculations). Finally, the vertical arrow and the thick line above the asymptotic limit shows the photon energy.

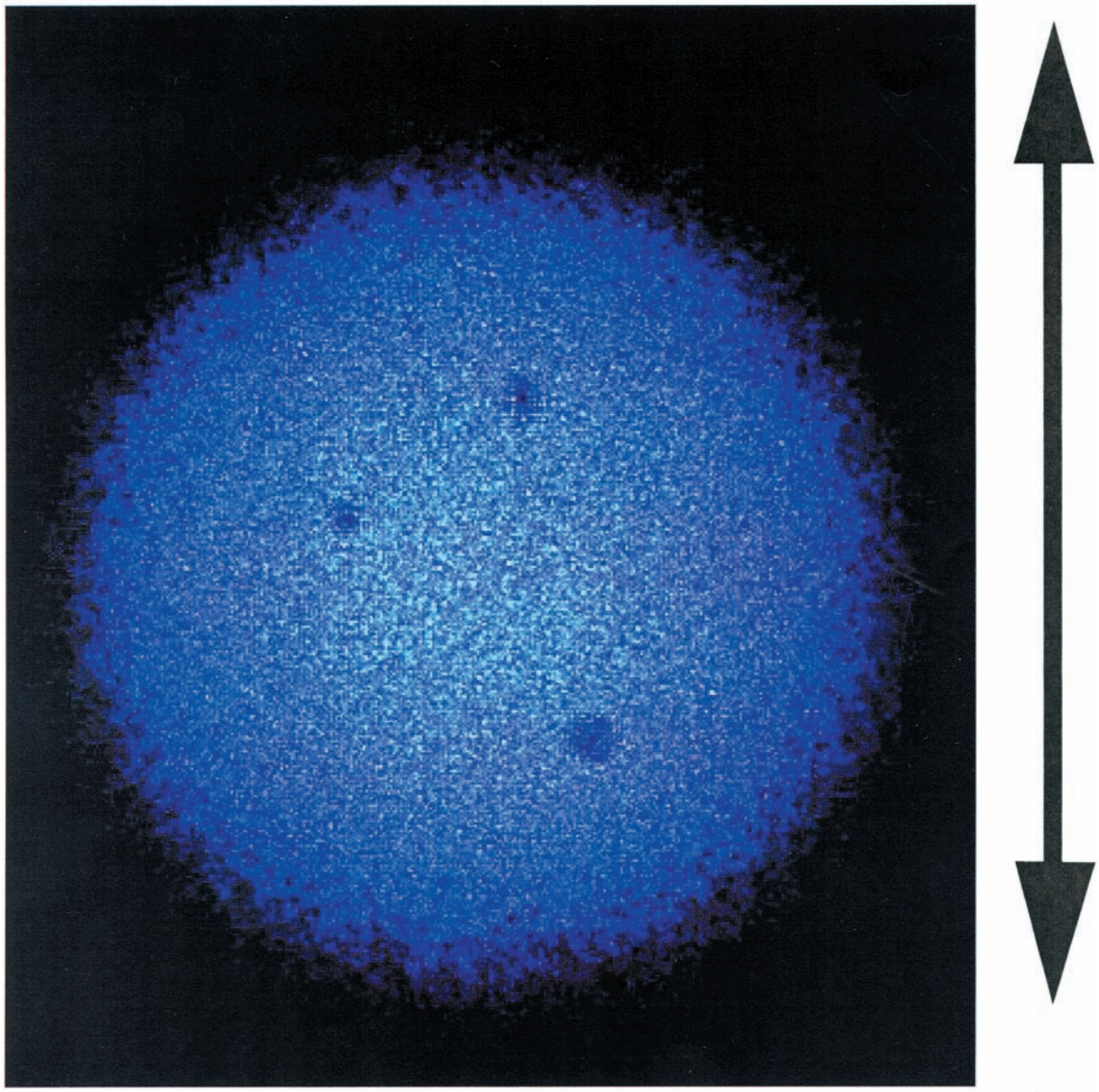

Figure 4. O^+ ion image for O_2-cyclohexane dissociated at 226 nm. The arrow shows the polarization of the photolysis/probe laser. The three spots are areas on the detector with lower sensitivity (see discussion in text).

IV. Results and Analysis

We confirm that the observed signal depends on the nozzle backing pressure (no signal was observed until the nozzle backing pressure was around 30 psig indicating that the formation of the X_2-Cy clusters is favored by a cold beam). Furthermore, heating the nozzle to 130 °C at a backing pressure of 50 psig destroys the observed signal. The cyclohexane concentration was varied by cooling the reservoir to discriminate against higher order clusters. Furthermore, we confirmed that the observed O-atom or Cl-atom signal vanished completely when the cyclohexane bubbler is bypassed and only a Cl_2/He or O_2/He mixture is introduced into the chamber. These observations provide strong evidence that the observed signal results from vdW clusters (X_2-Cy_n) but does not result from higher order ($n > 1$) clusters. Furthermore, fragmentation of higher order clusters should produce atoms with low kinetic energies affecting only the low energy portion of the resulting translational energy distribution and not the high energy tail used for energetic analysis.

A. O_2-Cyclohexane. Figure 4 shows the O^+ ion image obtained for O_2-cyclohexane dissociated at 226 nm with a vertically polarized laser as shown. The angular distribution of the photofragments is completely isotropic. The three spots apparent in the image result from less sensitive areas of the imaging detector. The O_2-Cy data is analyzed in a manner similar to that of Yoder et al.[26] To fit these data, we have averaged all data points equidistant from the center of the image to generate a radial intensity distribution (Figure 5 inset). This radial intensity distribution is then fit to a sum of four Gaussian functions. The coefficients and exponential terms for these functions are given in Table 2. The Gaussian fitting functions are then analytically inverse-Abel transformed to give the product intensity distribution as a function of distance from the center-of-mass of the dissociating complex. We convert the intensity distribution to a velocity distribution and then into a center-of-mass recoil kinetic energy distribution, $P(E_T)$, accounting for the dE/dv differential term in the transformation from the velocity distribution to energy distribution. The total recoil kinetic energy distribution, shown in Figure 5, is derived under the assumption of an O-atom recoil from a 100 amu partner (cyclohexane + O). We cannot confirm this dissociation mechanism since no signal at $m/e = 100$ is observed to

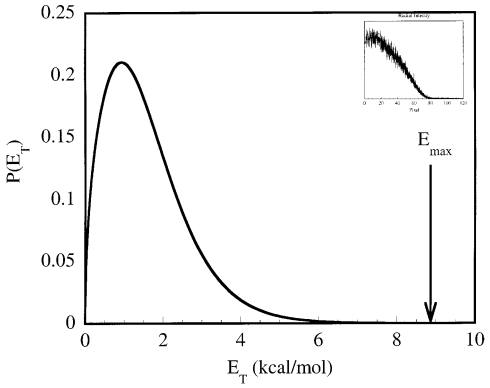

Figure 5. $P(E_T)$ for O_2−cyclohexane dissociated at 226 nm. The arrow shows the calculated energetic limit for dissociation of the cluster.

TABLE 2: Parameters Used to Fit the O_2−Cyclohexane Radial Intensity Distribution to the Gaussian Function: $f(x) = \sum_i C_i \exp[-(x/\sigma_i)^2]$

i	C_i	σ_i
1	0.01261	1050
2	0.03242	561.9
3	−0.03807	703.7
4	−0.006057	373.9

momentum match with the observed $m/e = 16$ signal. However, this assumption serves as a starting point to compare with the expected energetics for this cluster.

B. Cl_2−Cyclohexane. Figure 6 shows the $Cl^*(^2P_{1/2})$ ion image from the dissociation of the Cl_2−cyclohexane vdW cluster at 240 nm. We have acquired the ion image for $Cl(^2P_{3/2})$ from the dissociation of these clusters at 241 nm. The image is nearly identical to that observed for $Cl^*(^2P_{1/2})$ but with a much lower signal-to-noise ratio due to the poor line strength for the 2 + 1 REMPI of $Cl(^2P_{3/2})$. The most obvious feature of this image is the anisotropic distribution of Cl fragments. This result immediately suggests that the dynamics of the dissociation differ for the O_2−Cy and Cl_2−Cy clusters. The ion image is fit using the BASEX[27] set of programs. The resulting speed distribution for the Cl atom is then converted into a translational energy distribution in the center-of-mass reference frame using the limiting assumption of Cl recoiling from a Cl−cyclohexane cluster; again this assumption will not correctly model secondary dissociation, but it provides a limiting case for the analysis of the primary fragmentation channel. We give the resulting $P(E_T)$ in Figure 7 and the velocity-dependent anisotropy parameter in Figure 8.

Finally, we determine the $Cl^*(^2P_{1/2})/Cl(^2P_{3/2})$ branching ratio in the following manner. A molecular beam of 5% Cl_2 in He is introduced into the vacuum chamber and photolyzed at the interaction region using 425-nm photons (vertically polarized). Within the 10-ns laser pulse we photolyze and probe the nascent $Cl^*(^2P_{1/2})$ and $Cl(^2P_{3/2})$ atoms. At this wavelength Cl_2 dissociates to give $Cl^*(^2P_{1/2}) + Cl(^2P_{3/2})$ products with a Cl product angular distribution parallel to the laser polarization axis.[23] Integrating the total observed signal between ±12.5° of vertical (along the laser polarization axis) allows for a calibration of the experimental efficiency using the relation

$$\left(\frac{Cl^*(^2P_{1/2})}{Cl(^2P_{3/2})}\right)_{true} = \xi_{det}\left(\frac{Cl^*(^2P_{1/2})}{Cl(^2P_{3/2})}\right)_{meas} \quad (6)$$

where $[Cl^*(^2P_{1/2})/Cl(^2P_{3/2})]_{meas}$ is the ratio of the relative intensities, ξ_{det} (= 13.9) is the detection efficiency (a function of the REMPI line strengths for $Cl^*(^2P_{1/2})$ and $Cl(^2P_{3/2})$), and $[Cl^*(^2P_{1/2})/Cl(^2P_{3/2})]_{true}$ is the true branching ratio (1:1 for this dissociation channel in Cl_2).[23] The $Cl^*(^2P_{1/2})/Cl(^2P_{3/2})$ branching ratio from the dissociation of the clusters is found to be $[Cl^*(^2P_{1/2})/Cl(^2P_{3/2})] = 0.53 \pm 0.05$. Finally, since we detect both ground-state $Cl(^2P_{3/2})$ and spin−orbit excited $Cl^*(^2P_{1/2})$, the spin−orbit energy (0.109 eV = 2.5 kcal/mol)[23] of Cl could impact the observed $P(E_T)$. However, there is no significant difference in the observed $P(E_T)$ for the two spin−orbit states.

V. Discussion

A. O_2−Cyclohexane. The only available mechanism for dissociation for O_2−cyclohexane at this wavelength is a dissociation following conversion to the neutral excited states of O_2 through transfer of an electron to cyclohexane since, according to Figure 2, the charge-transfer state of O_2−Cy is strongly bound at this dissociation wavelength. One can consider how dissociation on these states compares with the observed $P(E_T)$. First, the energetic limit for dissociation on the neutral excited states is calculated to be 8.8 kcal/mol ($E_{avail} = E_{photon} - D_0(O_2)$). This energetic limit is given by the position of the arrow in Figure 5. The observed $P(E_T)$ fits within this limit. Furthermore, the observed ion image for O^+ from O_2−cyclohexane dissociation, Figure 4, is completely isotropic. Furthermore, the recoil kinetic energy distribution peaks at very low energy (∼2 kcal/mol) indicating dissociation on a state with a small barrier in the exit channel.

Other workers[6,10] have noted that the fast channel from I_2−benzene photodissociation is consistent with the recoil of an uncaged I atom from an oblique geometry while the slow channel is consistent with dissociation of caged I atoms (those that recoil into the ring). We now consider if our data for O_2−cyclohexane provides any indication if the dissociation takes place from either the axial structure (Figure 1a) or the resting structure (Figure 1b). If the dissociation were to result from the axial structure, then we would expect to see two distinct O atom kinetic energy distributions with dissimilar angular distributions provided (1) secondary dissociation (of the O−cyclohexane cluster) occurs in less than the laser pulse-width (∼10 ns), and (2) no large amplitude motions (e.g., O_2 torsion) significantly distort the axial symmetry of the cluster. On the other hand, both O atoms experience similar environments in the resting structure (Figure 1b). Though not equivalent, both are caged by the nearby cyclohexane ring during a dissociation. Therefore, dissociation from the resting structure should give an isotropic O atom angular distribution (from caging effects) with both O atoms experiencing similar recoil energies from the cluster since (neglecting molecular rotation) both O atoms essentially recoil from one another. The data seems more consistent with dissociation from resting O_2−cyclohexane, Figure 1b, which is the more strongly bound cluster according to our ab initio calculations. However, we cannot completely discount dissociation from an axial O_2−Cy cluster (Figure 1a) undergoing large amplitude motion in the ground-state contributing to part of the observed signal.

B. Cl_2−Cyclohexane. The Cl^+ ion image shows a clearly anisotropic distribution which, at least for the highest translational energy fragments, peaks along the laser polarization axis. The velocity-dependent anisotropy parameter, shown in Figure 8, rises from $\beta \sim 0$ for the lowest velocity fragments to around $\beta \sim 1.7-2$ for the highest velocity fragments. Clearly, at least two Cl atom channels are required to explain this result. We follow the method of Potter et al.[28] to extract the velocity distributions for two channels with assumed anisotropy parameters of $\beta = 0.08$ (the value for the slowest fragments) and

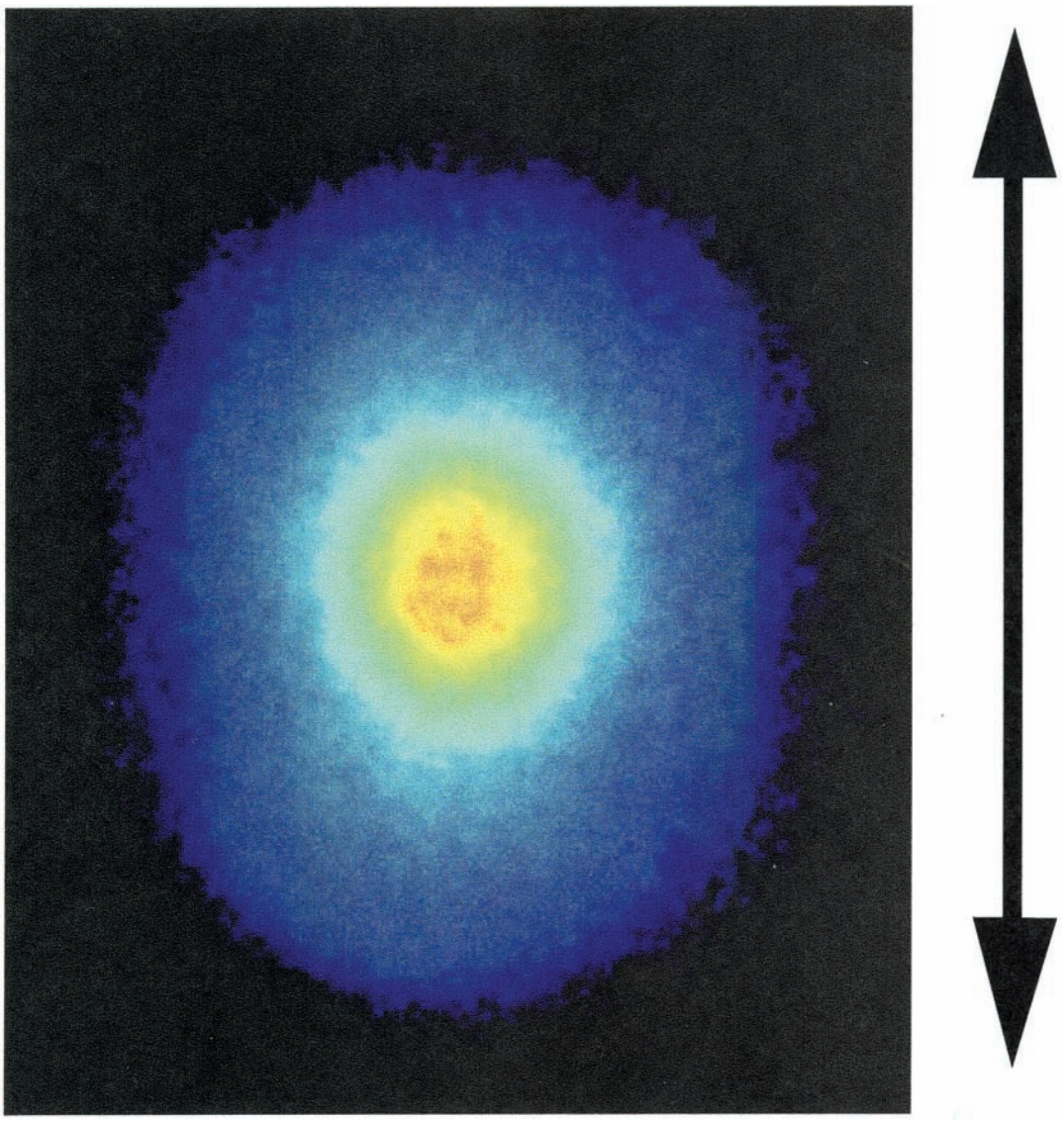

Figure 6. Cl^{*+} ion image for Cl_2-cyclohexane dissociated at 240 nm. The arrow shows the polarization of the photolysis/probe laser.

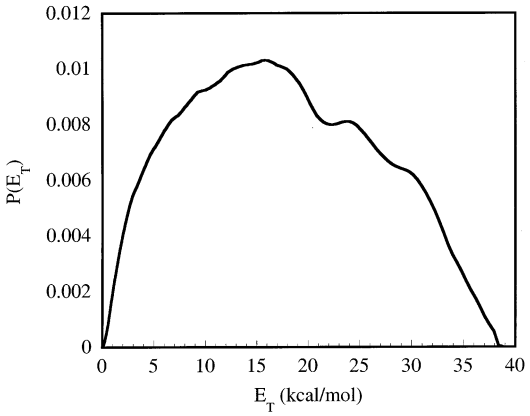

Figure 7. $P(E_T)$ for Cl_2-Cy dissociated at 240 nm.

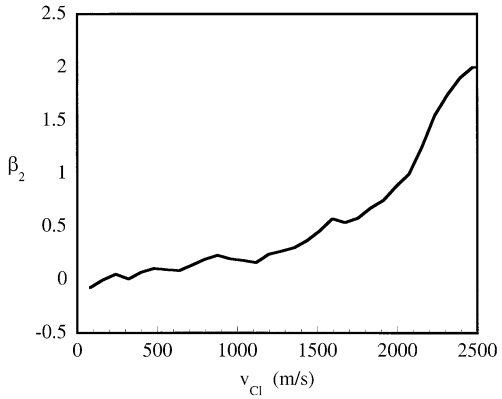

Figure 8. Velocity-dependent Cl angular distribution extracted from the Cl ion image (Figure 7) using the BASEX set of programs.

$\beta = 2$ (the value for the fastest fragments) from the total velocity distribution and the velocity-dependent anisotropy parameter (Figure 8). Figure 9 (top) gives the recoil kinetic energy distribution for the fast, highly anisotropic channel ($\beta = 1.7-2$) derived from the extracted velocity distribution. We again derived $P(E_T)$ assuming Cl recoiling from a Cl−cyclohexane cluster. Figure 10 shows the velocity distribution for the slow, isotropic channel ($\beta \sim 0$). We do not give the resulting $P(E_T)$ for this channel but instead fit it to a Boltzmann speed distribution since, as will be discussed later in this section, this distribution corresponds to Cl atoms from secondary dissociation.

We now consider if the recoil kinetic energy distribution from Cl_2-cyclohexane is consistent with dissociation on the charge-transfer state or the neutral excited states of Cl_2 following reverse electron transfer. The energetic limit for dissociation on the

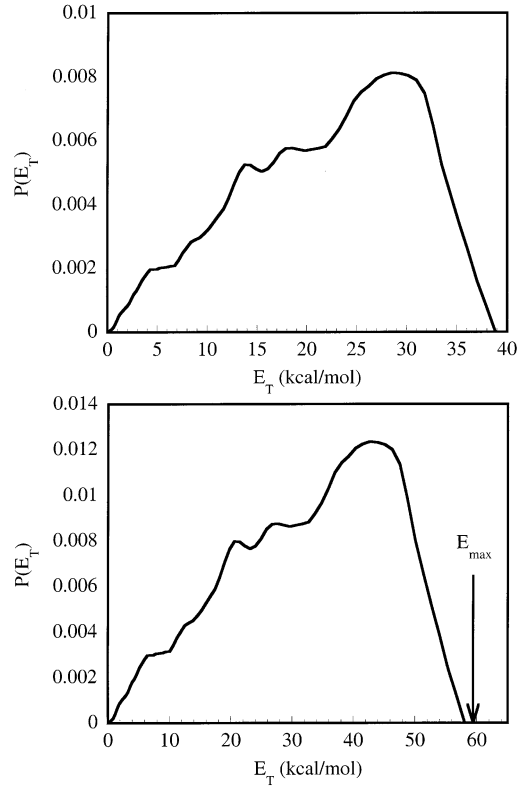

Figure 9. (Top) $P(E_T)$ for the fast anisotropic Cl atom channel assuming dissociation from a strongly interacting cluster. The reduced mass used in the determination of this $P(E_T)$ is that for Cl recoiling from a 119 amu partner (Cl−Cy cluster). (Bottom) $P(E_T)$ for the fast anisotropic Cl atom channel assuming dissociation from a weakly interacting cluster. The reduced mass used in the determination of this $P(E_T)$ is that for Cl recoiling from another Cl atom. The arrow marks the maximum available energy in the center-of-mass reference from for a dissociation yielding $Cl(^2P_{3/2}) + Cl^*(^2P_{1/2})$.

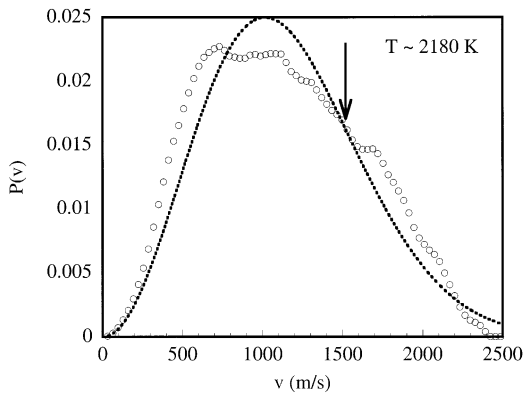

Figure 10. $P(v)$ for the slow, isotropic Cl atom channel. A reasonable fit to the $P(v)$ is found using a Maxwell−Boltzmann distribution at a temperature of 2180 K.

neutral excited states of Cl_2 may be calculated as $E_{avail} = E_{photon} - D_0(Cl_2) - E_{SO}(Cl) = 59.5$ kcal/mol where E_{SO} is the spin−orbit energy of Cl (2.5 kcal/mol). To calculate the energetic limit for the dissociation of the charge-transfer state we estimate the energetics for the ionic cluster formed from the harpooning reaction in the exit channel (Cy^+−Cl^-) by approximating close contact between Cy^+ and Cl^-. The ionic radius of Cl^- is 1.8 Å, so we consider spherical Cl^- in contact with the Cy ring. The point of closest contact between the box and the ring is when the box encounters the H atoms. This separation is 3.2 Å (Cl^- ionic radius + C−H bond length + H covalent radius). We approximate the energy of this ionic cluster using eq 1 along with the ionization potential of cyclohexane and the electron affinity of Cl (3.6 eV)[29] and find the energy for the Cy^+−Cl^- products $E_{CT}(Cy^+-Cl^-) = 2.1$ eV. The energy of the cluster lies above the asymptotic limit of the ground state by ~0.5 eV (49 kcal/mol), giving the available energy as $E_{avail} = E_{photon} - D_0(Cl_2) - E_{CT}(Cy^+-Cl^-) = 0.55$ eV or 13 kcal/mol. This model provides only a rough estimate of the available energy and this is an *upper limit* to the available energy since any greater separation than close contact requires more energy be deposited into the ionic product cluster.

Insight into the dissociation mechanism may be provided by a comparison of the energetic limits outlined in the previous paragraph with the total kinetic energy distribution (Figures 7 and 9) and the kinetic energy distribution for the fast dissociation channel. First, the limit for dissociation on the charge-transfer state (13 kcal/mol) clearly disagrees with either the total $P(E_T)$ or the $P(E_T)$ derived for either Cl atom channel. The limit for dissociation on the neutral excited states of Cl_2 (following reverse electron transfer) agrees with the observed total $P(E_T)$, or the $P(E_T)$ for the fast dissociation channel or the $P(v)$ for the slow channel. However, the sharp cutoff in the $P(E_T)$ suggests a firm energetic limit. Figure 9 (bottom) shows the $P(E_T)$ derived from the velocity distribution for the fast channel assuming Cl recoiling from another Cl atom (no interaction with the cyclohexane ring, we discuss the implication of these kinematics latter in this section). This observation provides strong evidence that the dissociation does not take place on the initially accessed charge-transfer state but rather after a non-adiabatic hop to one of the neutral excited states of Cl_2 (we discuss the implications of this in more detail later). Thus, we assign the fast, anisotropic Cl atoms to prompt dissociation following fast electron transfer (presumably with a time scale similar to that of I_2−benzene, ~200 fs [6]).

The slow, isotropic distribution cannot be assigned so easily; it cannot result entirely from dissociation on the charge-transfer state since an available energy of 13 kcal/mol corresponds to a velocity of 1550 m/s for primary Cl atoms, well below the limit of the speed distribution. This speed distribution is reasonably well fit with a Maxwell−Boltzmann distribution with $T_{trans} = 2180$ K. The isotropic distribution indicates these Cl atoms result from dissociation on a long time scale relative to molecular rotation.

By taking a ratio of the integrated area for the $P(v)$ from the slow distribution and the total $P(v)$ determined from the image, we find that 69% of the signal corresponds to the slow, isotropic distribution with the remaining 31% due to dissociation on the neutral excited states (the fast, anisotropic channel). Obviously, the slow distribution contains several channels. We assume that the slow distribution is a linear combination of secondary Cl atoms resulting from dissociation on the neutral excited states as well as primary and secondary Cl atoms from dissociation on the charge-transfer state and that one secondary Cl atom is formed for each primary Cl atom from either dissociation mechanism. Thus, 31% of the Cl atoms result from secondary dissociation on the neutral excited states and 38% result from the combination of primary and secondary charge-transfer dissociation. Thus, 38% of the total dissociation could take place through the charge-transfer state. This value represents a lower limit since the assumption of forming one secondary Cl atom for each primary is suspect but allows for an unambiguous determination of a limit for dissociation on the charge-transfer state. When this analysis is applied to the velocity distribution obtained on resonance with $Cl(^2P_{3/2})$ we find 31% of the observed Cl atoms result from the fast channel (primary

TABLE 3: Electronic Configuration for Low-Lying Neutral Excited States of Cl_2 Taken from ref 24. The Electronic Configuration Is Given near the Cl−Cl Bond Length Corresponding to the Franck−Condon Region of the Charge-Transfer State and at a Cl−Cl Separation of $6a_0$

state	Franck−Condon	r(Cl−Cl) = $6a_0$
$1^{1,3}\Pi_u$	$\sigma_g^2\pi_u^4\pi_g^3\sigma_u^1$	$\sigma_g^1\pi_u^3\pi_g^4\sigma_u^2$(59%)
$1^{1,3}\Pi_g$	$\sigma_g^2\pi_u^3\pi_g^4\sigma_u^1$	$\sigma_g^1\pi_u^4\pi_g^3\sigma_u^2$(54%)
$1^3\Sigma_u^+$	$\sigma_g^1\pi_u^4\pi_g^4\sigma_u^1$	NC
$1^3\Sigma_g^-$	$\sigma_g^2\pi_u^4\pi_g^2\sigma_u^2$	$\sigma_g^2\pi_u^2\pi_g^4\sigma_u^2$(40%)
$1^1\Delta_g$	$\sigma_g^2\pi_u^4\pi_g^2\sigma_u^2$	$\sigma_g^2\pi_u^2\pi_g^4\sigma_u^2$(40%)
2^1	$\Sigma_g^+\ \sigma_g^2\pi_u^4\pi_g^2\sigma_u^2$	$\sigma_g^2\pi_u^2\pi_g^4\sigma_u^2$(40%)
1^1	$\Sigma_u^-\ \sigma_g^2\pi_u^3\pi_g^3\sigma_u^2$	NC
$1^3\Delta_u$	$\sigma_g^2\pi_u^3\pi_g^3\sigma_u^2$	NC
2^3	$\Sigma_u^+\ \sigma_g^2\pi_u^3\pi_g^3\sigma_u^2$	NC

dissociation on the neutral excited state) giving 38% of the observed Cl from dissociation on the charge-transfer state. These results compare with the determination of Cheng et al.[6] for the I_2−Bz system that about 10% of the total dissociation occurs through the charge-transfer state.

For I_2−Bz, Zewail and co-workers[6] observed a large fraction of dissociation resulting from a nonadiabatic transition to the neutral excited states of I_2. A similar mechanism very likely results in the dissociation of the Cl_2−cyclohexane after funneling onto the neutral excited states through an avoided crossing with the initially accessed charge-transfer state. We consider why the avoided crossing between the initially accessed charge-transfer state and the neutral excited states of Cl_2 might be strong. In the Cl_2 point group, $D_\infty h$, the electronic configuration of the anionic ground state ($^2\Sigma_u^+$) is $\sigma_g^2\pi_u^4\pi_g^4\sigma_u^1$ (neglecting core electrons). Our plot of the charge-transfer state, shown in Figure 3, indicates that two states cross the charge-transfer state in the Franck−Condon region: $1^3\Pi_u$ and $1^1\Pi_u$. According to Kokh et al.,[24] the electronic configuration of both states in the Franck−Condon region is $\sigma_g^2\pi_u^4\pi_g^3\sigma_u^1$. These states are derived from the charge-transfer state by a loss of a single electron (π_g). Butler and co-workers[30−32] have shown several cases where a molecular dissociation is strongly influenced by hopping between surfaces coupled by a one-electron change matrix element. According to Figure 3, all other avoided crossings between the charge-transfer state and the neutral excited states of Cl_2 occur much farther out in the exit channel ($\sim 6a_0$). We give the electronic configurations for the various neutral excited states from Kokh et al. in Table 3 for r(Cl−Cl) = $6a_0$. Several states maintain the same dominant electronic configuration at r(Cl−Cl) = $6a_0$, these are marked with NC (no change). For those states with a significant contribution from another electronic configuration, we gives its percentage at $r = 6a_0$ in Table 3. Only three states of the neutral excited state of Cl_2 have a dominant electronic configuration that differs from the ground state of the negative ion by a one-electron change. These, too, may couple quite strongly with the initially accessed excited state through a one-electron change matrix element. Young and co-workers[14] invoked an analogous mechanism in the dissociation of O_2−alkenes at 226 nm where O_2^- $3\sigma_g^2 1\pi_u^4 1\pi_g^3$ returns an electron to the cation resulting in O_2* $\sigma_g^2\pi_u^3\pi_g^3$.

Finally, we consider if the observed data for the Cl_2−cyclohexane cluster is consistent with dissociation from the predicted van der Waals cluster (Figure 1c). As was mentioned before, others have concluded that the anisotropic distribution for the fast I atoms from I_2−benzene results from a cluster with a near axial structure.[6,10] The fast Cl atoms from Cl_2−cyclohexane exhibit a very anisotropic angular distribution approaching the limiting value ($\beta \sim 1.7-2$) consistent with the expectation from a prompt dissociation of an axial cluster. This result indicates the Cl_2 cluster has a tighter potential along the wag coordinate in the vdW ground state. Figure 9 shows the predicted $P(E_T)$ for dissociation under two limiting cases: Cl recoiling from a Cl−Cy cluster (strong interaction with the ring) and Cl recoiling from the other Cl atom (no interaction with the ring). The fact that Figure 9 (bottom) agrees quite well with the maximum available energy for a dissociation yielding Cl*($^2P_{1/2}$), 59.5 kcal/mol, means a significant fraction of the primary dissociation on the neutral excited state (the fast, anisotropic channel) results from a cluster geometry with a weak Cl_2 ring interaction probably due to large separation between the subunits. The cluster most likely samples a large number of geometries ranging from those with significant interactions between the subunits (Figure 9, top) and those with almost no interaction between the subunits (Figure 9, bottom). Therefore, the reduced mass used in the determination of the $P(E_T)$ changes continuously over the full range of geometries.

VI. Conclusions

The dissociation of O_2−cyclohexane clusters at 226 nm results in the production of O(^3P_j) while the dissociation of Cl_2−cyclohexane at 240 nm results in the production of Cl($^2P_{3/2}$) and Cl*($^2P_{1/2}$). For O_2−cyclohexane, the product distribution is isotropic and the recoil kinetic energy distribution is peaked near 2 kcal/mol. Furthermore, the recoil kinetic energy distribution agrees with the expected energetic limit for dissociation on the neutral excited states of O_2. We therefore, consider this mechanism the most likely for the dissociation of these clusters. The isotropic O atom angular distribution and the unimodal velocity distribution provide strong evidence that the dissociation takes place from the resting type structure (Figure 1b), which is the predicted global minimum. For Cl_2−cyclohexane, the energetics allow for the dissociation to take place on the initially accessed charge-transfer state via a mechanism in which the cyclohexane cation harpoons Cl^- in the exit channel while the other Cl-atom recoils from the heavier fragment. However, the recoil kinetic energy distribution is not consistent with this mechanism. The velocity dependence of the angular distribution indicates that Cl is formed through at least two channels. Assuming the total velocity distribution is a sum of two independent velocity distributions, we derive a velocity distribution for a fast, anisotropic channel that corresponds to dissociation of the Cl_2−cyclohexane cluster following a nonadiabatic hop to the neutral excited states of Cl_2, and we derive a velocity distribution for a slow, isotropic channel corresponding to secondary dissociation with a translational temperature of about 2180 K. Analysis of the relative populations for the slow, isotropic distribution and the fast, anisotropic channel reveals that about 62% of the Cl atoms result from dissociation on the neutral excited states and 38% result from dissociation of the initially accessed charge-transfer state. This dissociation occurs from an axial cluster derived from the initial ground-state van der Waals cluster, resulting in a nonstatistical $P(E_T)$ due to the large reverse barrier in the exit channel. The reduced mass used in the determination of the $P(E_T)$ depends quite strongly on the subunit separation for the dissociating cluster. The rapid relaxation of these systems to the neutral excited states results from a one-electron change through one of many avoided crossings with repulsive neutral excited states of the diatomic electron acceptor. Indeed, this mechanism is the key to the dissociation of these systems since (as pointed out by Young and co-workers[14]) this one-electron change need not involve the initially donated electron. Therefore, the cluster typically ends up on a purely repulsive state where rapid dissociation of the diatom results in atomic product formation.

Acknowledgment. B. Parsons thanks Dr. David Osborn for a useful discussion of negative ion energetics, Prof. Hanna Reisler for the donation of the BASEX set of programs used in the analysis of the Cl_2−cyclohexane system, and Dr. D. Kokh for the plot of the neutral excited states of Cl_2 correlating with 2 Cl(^{2}P) fragments. We gratefully acknowledge the assistance of Mr. Mark Jaska. Sandia is a multiprogram laboratory operated by Sandia Corporation, a Lockheed Martin Company, for the U.S. Department of Energy's National Nuclear Security Administration under contract DE-AC04-94AL85000.

References and Notes

(1) Bensei, H. A.; Hildebrand, J. H. *J. Am. Chem. Soc.* **1949**, *71*, 2703.
(2) Lang, F. T.; Strong, R. L. *J. Am. Chem. Soc.* **1965**, *87*, 2345.
(3) Mulliken, R. S. *J. Am. Chem. Soc.* **1952**, *74*, 811.
(4) Turro, N. J. *Modern Molecular Photochemistry*; University Science Books: Sausalito, CA, 1991.
(5) Cheng, P. Y.; Zhong, D.; Zewail, A. H. *J. Chem. Phys.* **1995**, *103*, 5153.
(6) Cheng, P. Y.; Zhong, D.; Zewail, A. H. *J. Chem. Phys.* **1996**, *105*, 6216.
(7) DeBoer, G.; Young, M. A. *J. Chem. Phys.* **1997**, *106*, 5468.
(8) Granucci, G.; Persico, M. *Chem. Phys. Lett.* **1993**, *205*, 331.
(9) DeBoer, G.; Burnett, J. W.; Young, M. A. *Chem. Phys. Lett.* **1996**, *259*, 368.
(10) DeBoer, G.; Burnett, J. W.; Fujimoto, A.; Young, M. A. *J. Phys. Chem.* **1996**, *100*, 14882.
(11) Cheng, P. Y.; Zhong, D.; Zewail, A. H. *Chem. Phys. Lett.* **1995**, *242*, 369.
(12) Grover, J. R.; Hagenow, G.; Walters, E. A. *J. Chem. Phys.* **1992**, *97*, 628.
(13) Maslen, P. E.; Papanikolas, J. M.; Faeder, J.; Parson, R.; O'Neil, S. V. *J. Chem. Phys.* **1994**, *101*, 5731.
(14) DeBoer, G.; Prince, A. P.; Young, M. A. *J. Chem. Phys.* **2001**, *115*, 3112.
(15) Guidoni, A. G.; Paladini, A.; Veneziani, M.; Naaman, R.; Di Palma, T. M. *Appl. Surf. Sci.* **2000**, *154*−*155*, 186.
(16) Frisch, M. J.; Trucks, G. W.; Schlegel, H. B.; Scuseria, G. E.; Robb, M. A.; Cheeseman, J. R.; Zakrzewski, V. G.; Montgomery, J. J. A.; Stratmann, R. E.; Burant, J. C.; Dapprich, S.; Millam, J. M.; Daniels, A. D.; Kudin, K. N.; Strain, M. C.; Farkas, O.; Tomasi, J.; Barone, V.; Cossi, M.; Cammi, R.; Mennucci, B.; Pomelli, C.; Adamo, C.; Clifford, S.; Ochterski, J.; Petersson, G. A.; Ayala, P. Y.; Cui, Q.; Morokuma, K.; Malick, D. K.; Rabuck, A. D.; Raghavachari, K.; Foresman, J. B.; Cioslowski, J.; Ortiz, J. V.; Stefanov, B. B.; Liu, G.; Liashenko, A.; Piskorz, P.; Komaromi, I.; Gomperts, R.; Martin, R. L.; Fox, D. J.; Keith, T.; Al-Laham, M. A.; Peng, C. Y.; Nanayakkara, A.; Gonzalez, C.; Challacombe, M.; Gill, P. M. W.; Johnson, B.; Chen, W.; Wong, M. W.; Andres, J. L.; Gonzalez, C.; Head-Gordon, M.; Replogle, E. S.; Pople, J. A. *Gaussian 98*, Rev. A.6 ed.; Gaussian, Inc: Pittsburgh, PA, 1998.
(17) Su, J. T.; Zewail, A. H. *J. Phys. Chem. A* **1998**, *102*, 4082.
(18) Bieri, G.; Burger, F.; Heilbronner, E.; Maier, J. P. *Helv. Chim. Acta* **1977**, *60*, 2214.
(19) Travers, M. J.; Cowles, D. C.; Ellison, G. B. *Chem. Phys. Lett.* **1989**, *164*, 449.
(20) Saxon, R. P.; Liu, B. *J. Chem. Phys.* **1977**, *67*, 5432.
(21) Nakatsuji, H.; Nakai, H. *Chem. Phys. Lett.* **1992**, *197*, 339.
(22) Bowen, K. H.; Liesegang, G. W.; Sanders, R. A.; Herschbach, D. W. *J. Phys. Chem.* **1983**, *87*, 557.
(23) Samartzis, P. C.; Bakker, B. L. G.; Rakitzis, T. P.; Parker, D. H.; Kitsopoulos, T. N. *J. Chem. Phys.* **1999**, *110*, 5201.
(24) Kokh, D. B.; Alekseyev, A. B.; Buenker, R. J. *J. Chem. Phys.* **2001**, *115*, 9298.
(25) Dojahn, J. G.; Chen, E. C. M.; Wentworth, W. E. *J. Phys. Chem.* **1996**, *100*, 9649.
(26) Yoder, L. M.; Barker, J. R.; Lorenz, K. T.; Chandler, D. W. *Chem. Phys. Lett.* **1999**, *302*, 602.
(27) Dribinski, V.; Ossadtchi, A.; Mandelshtam, V. A.; Reisler, H. *Rev. Sci. Instrum.* **2002**, *73*, 2634.
(28) Potter, A. B.; Dribinski, V.; Demyanenko, A. V.; Reisler, H. *Chem. Phys. Lett.* **2001**, *349*, 257.
(29) Berzinsh, U.; Gustafsson, M.; Hanstorp, D.; Klinkmuller, A.; Ljungblad, U.; Martensson-Pendrill, A. M. *Phys. Rev. A* **1995**, *51*, 231.
(30) Morton, M. L.; Szpunar, D. E.; Butler, L. J. *J. Chem. Phys.* **2001**, *115*, 204.
(31) Forde, N. R.; Morton, M. L.; Curry, S. L.; Wrenn, S. J.; Butler, L. J. *J. Chem. Phys.* **1999**, *111*, 4558.
(32) Butler, L. J. *Annu. Rev. Phys. Chem.* **1998**, *49*, 125.